

Posterior Sampling of Probabilistic Word Embeddings

Väinö Yrjänäinen*

Department of Statistics, Uppsala University

Isac Boström

Department of Mathematical Sciences,

Chalmers University of Technology

Måns Magnusson

Department of Statistics, Uppsala University

and

Johan Jonasson

Department of Mathematical Sciences,

Chalmers University of Technology

August 5, 2025

Abstract

Quantifying uncertainty in word embeddings is crucial for reliable inference from textual data. However, existing Bayesian methods such as Hamiltonian Monte Carlo (HMC) and mean-field variational inference (MFVI) are either computationally infeasible for large data or rely on restrictive assumptions. We propose a scalable Gibbs sampler using Polya-Gamma augmentation as well as Laplace approximation and compare them with MFVI and HMC for word embeddings. In addition, we address non-identifiability in word embeddings. Our Gibbs sampler and HMC correctly estimate uncertainties, while MFVI does not, and Laplace approximation only does so on large sample sizes, as expected. Applying the Gibbs sampler to the US Congress and the MovieLens datasets, we demonstrate the feasibility on larger real data. Finally, as a result of having draws from the full posterior, we show that the posterior mean of word embeddings improves over maximum a posteriori (MAP) estimates in terms of hold-out likelihood, especially for smaller sampling sizes, further strengthening the need for posterior sampling of word embeddings.

Keywords: Probabilistic Modeling, Markov Chain Monte Carlo, Bayesian statistics, Natural Language Processing, Gibbs sampling, Laplace Approximation

*The authors gratefully acknowledge support from the Wallenberg AI, Autonomous Systems and Software Program (WASP) funded by the Knut and Alice Wallenberg Foundation. The computations were enabled by resources provided by the National Academic Infrastructure for Supercomputing in Sweden (NAISS), partially funded by the Swedish Research Council through grant agreement no. 2022-06725.

1 INTRODUCTION

Word embeddings are vector representations of words that capture statistical relationships within textual data. Traditional word embedding methods, such as word2vec (Mikolov et al., 2013) and GloVe (Pennington et al., 2014), provide point estimates for each word, representing them as fixed vectors in a high-dimensional space. In recent years, word embeddings have been increasingly applied to inference tasks in the social sciences to investigate a wide range of linguistic and cultural aspects (Garg et al., 2018; Kozlowski et al., 2019; Rodman, 2020; Abramson et al., 2024). However, standard word embedding methods (e.g., word2vec and GloVe) do not quantify the uncertainty associated with the embeddings, which is essential for reliable inference and interpretation in scientific settings.

Probabilistic word embeddings (Rudolph et al., 2016; Bamler and Mandt, 2017) extend traditional word embedding and formulate word embeddings as a full probabilistic model. Nonetheless, quantifying uncertainty in these models poses significant challenges due to large datasets, non-identifiability, and large parameter spaces commonly involved in practical applications. An embedding model in typical settings can easily involve millions of parameters.

Antoniak and Mimno (2018) proposed bootstrap for embedding uncertainty estimation. However, bootstrap estimation of uncertainty requires orders of magnitude more computation than obtaining point estimates. More recently, Vallebueno et al. (2024) proposed a method for quantifying uncertainty in the GloVe embeddings. This approach estimates the uncertainty conditional on the context embedding parameters and hence does not provide a rigorous approach to uncertainty estimation. In addition, the approach does not work for low-frequency words, which often constitute the bulk of words in natural language (Piantadosi, 2014). In the Bayesian realm, Bamler and Mandt (2017) proposed mean-field variational inference (MFVI) for the estimation of word embeddings. Although computationally efficient, it is well known that MFVI underestimates posterior variance (Wang

and Blei, 2018), limiting its use in scientific settings. On the other hand, Hamiltonian Monte Carlo (HMC) can be used for embeddings but is usually not feasible due to the high computational cost. Thus, while there has been work on embedding uncertainty, accurate Bayesian uncertainty quantification of embeddings is still elusive.

In this paper, we present the following contributions:

1. We study the identifiability of word embeddings in the context of Bayesian inference and prove that current embeddings are not identified. Furthermore, we present a conceptually easy and computationally feasible way to identify the skip-gram with negative samples (SGNS), one of the two popular word2vec models and prove that this approach identifies the model.
2. We propose two new, computationally efficient algorithms for sampling embeddings: Laplace approximation and a Gibbs sampler. In addition, we compare with the gold-standard HMC on word embeddings.
3. We show that our proposed Gibbs sampler is more accurate than MFVI, and more computationally efficient than HMC for large models and data, a common setting in social science applications.

1.1 PROBABILISTIC WORD EMBEDDINGS

Probabilistic word embeddings (Rudolph et al., 2016; Bamler and Mandt, 2017; Rudolph and Blei, 2017) extend the standard SGNS word embedding model of (Mikolov et al., 2013) to a probabilistic model.

Let $\mathcal{D} = (w_i)_{i=1}^N$ denote a dataset consisting of a sequence of words, where each word w_i belongs to the *vocabulary* $W = \{1, \dots, V\}$, the set of all relevant words in the corpus.¹

¹Throughout the article, we use an implicit mapping from the set of words $W = \{\text{word0}, \text{word1}, \dots\}$ onto indices $\{1, \dots, V\}$, e.g. $\{\text{dog} \mapsto 1, \text{cat} \mapsto 2, \text{cow} \mapsto 3\}$. Hence, the word vector ρ_v for word $v \in W$ is just the v th column of the matrix ρ . The numeric indices have no meaning in word embeddings and thus

For each word $w \in W$ we associate two embedding vectors: A *target vector* $\rho_w \in \mathbb{R}^K$ and a *context vector* $\alpha_w \in \mathbb{R}^K$, where K denotes the dimensionality of the embedding. We organize the embeddings vectors into matrices such that $\rho \in \mathbb{R}^{V \times K}$ is the matrix of target vectors and $\alpha \in \mathbb{R}^{V \times K}$ the matrix of context vectors:

$$\rho = \begin{bmatrix} (\rho_1)^\top \\ (\rho_2)^\top \\ \vdots \\ (\rho_V)^\top \end{bmatrix}, \quad \alpha = \begin{bmatrix} (\alpha_1)^\top \\ (\alpha_2)^\top \\ \vdots \\ (\alpha_V)^\top \end{bmatrix}. \quad (1)$$

The complete set of parameters $\theta \in \mathbb{R}^{2V \times K}$ is then defined as

$$\theta = \begin{bmatrix} \rho \\ \alpha \end{bmatrix}. \quad (2)$$

The SGNS likelihood nicely factors into terms, where each term only has a handful of parameters:

$$\log p(\mathcal{D} \mid \theta) = \sum_{i=1}^N \left(\underbrace{\sum_{v \in C_i^+} \log \sigma(\rho_{w_i}^\top \alpha_v)}_{\text{positive samples}} + \underbrace{\sum_{v \in C_i^-} \log(1 - \sigma(\rho_{w_i}^\top \alpha_v))}_{\text{negative samples}} \right) \quad (3)$$

where C_i^+ is the context window, or the set of positive samples, for word w_i at index i in the data. Specifically, the context window is the set of words within the distance $M \in \mathbb{N}$ from the center word, i.e.

$$C_i^+ = \{w_{i-M}, \dots, w_{i-1}, w_{i+1}, \dots, w_{i+M}\}. \quad (4)$$

For each positive sample, $n_s \in \mathbb{N}$ negative samples forming C_i^- are drawn randomly from the empirical distribution of all words in W , sometimes with slight adjustments (Mikolov et al., 2013). It can further be computationally and conceptually beneficial to formulate the likelihood as a sum over word pairs,

$$\log p(\mathcal{D} \mid \theta) = \sum_{(w,v) \in W \times W} \left(n_{wv}^+ \log \sigma(\rho_w^\top \alpha_v) + n_{wv}^- \log(1 - \sigma(\rho_w^\top \alpha_v)) \right). \quad (5)$$

no information is lost.

Here, n_{wv}^+ and n_{wv}^- denotes the number of times that (w, v) appear in the positive and negative samples.

A common prior for the embedding vectors is a spherical Gaussian prior

$$\begin{aligned}\rho_w &\sim \mathcal{N}(0, \lambda^{-1} \mathbf{I}), \quad w \in W, \\ \alpha_w &\sim \mathcal{N}(0, \lambda^{-1} \mathbf{I}), \quad w \in W\end{aligned}\tag{6}$$

where $\lambda \in \mathbb{R}_+$ is a hyperparameter. Other priors used for embedding vectors, and common in practical applications, include dynamic priors (Rudolph and Blei, 2017; Bamler and Mandt, 2017), grouped priors (Rudolph et al., 2017), and informative priors focused on interpretability (Bodell et al., 2019), and graph priors (Yrjänäinen and Magnusson, 2022), most of which are Gaussian.

2 IDENTIFICATION OF THE PROBABILISTIC SGNS MODEL

The SGNS likelihood in Equation 3 only consists of dot products between the target vectors ρ_w and the context vectors α_v . Because dot products are preserved under invertible linear transformations, we can apply the following transformations for any invertible matrix \mathbf{A} in the general linear group of degree K , denoted $\text{GL}(K)$, i.e., $\mathbf{A} \in \text{GL}(K)$:

$$\rho'_w = \mathbf{A}\rho_w, \quad \alpha'_v = \mathbf{A}^{-\top}\alpha_v. \tag{7}$$

Under these transformations the dot product is invariant, $(\rho'_w)^\top \alpha'_v = (\rho_w)^\top \alpha_v$, and the likelihood remains unchanged. As a result, there are $K \times K$ degrees of freedom corresponding to these transformations that do not affect the likelihood. This makes the SGNS model non-identifiable in the sense that the mapping from the parameter space onto likelihoods is not one-to-one (Bickel and Doksum, 2015).

Mu et al. (2019) propose adding L_2 regularization to identify the likelihood. However, their proof only shows that the MAP estimate is unique up to a rotation. The likelihood

still retains *orthogonal* symmetries $p(\theta \mid x) = p(\theta \mathbf{O} \mid x)$, where $\mathbf{O}^\top \mathbf{O} = \mathbf{I}$. Thus, Mu et al.'s (2019) method does not properly identify the likelihood. Instead, this results in the posterior distribution exhibiting a *spherical-shell* like structure, where even a very concentrated posterior will be distributed on the shell of a hypersphere, see Figure 1. Intuitively one might view this as any orientation of the embeddings is valid.

Fixing K^2 elements of α eliminates these symmetries. We consider θ for which the K first context vectors, α_I , where $I = \{1, \dots, K\}$, form a fixed and predetermined invertible matrix $\mathbf{M} \in \mathbb{R}^{K \times K}$, while the rest of the context vectors form an unrestricted matrix $\alpha_J \in \mathbb{R}^{(V-K) \times K}$, $J = \{K+1, \dots, V\}$. In Proposition 1, we show that the restricted model can represent any likelihood that the unrestricted model can, and in Proposition 2 we show that the likelihood of the restricted model is identifiable.

Proposition 1. *Given any embedding $\hat{\alpha}, \hat{\rho}$, and any invertible matrix $\mathbf{M} \in \mathbb{R}^{K \times K}$, the following embedding*

$$\rho = \hat{\rho}(\hat{\alpha}_I^{-1} \mathbf{M})^{-\top}, \quad \alpha = \begin{bmatrix} \mathbf{M} \\ \hat{\alpha}_J \hat{\alpha}_I^{-1} \mathbf{M} \end{bmatrix} \quad (8)$$

has the same likelihood

$$p(\mathcal{D} \mid \rho, \alpha) = p(\mathcal{D} \mid \hat{\rho}, \hat{\alpha}) \quad (9)$$

for any dataset \mathcal{D} .

Proof in Appendix A.

Proposition 2. *Given any invertible matrix $\mathbf{M} \in \mathbb{R}^{K \times K}$, any two embeddings $\alpha = \begin{bmatrix} \mathbf{M} \\ \alpha_J \end{bmatrix}$, ρ and $\alpha' = \begin{bmatrix} \mathbf{M} \\ \alpha'_J \end{bmatrix}$, ρ' , for which $\alpha \neq \alpha'$ or $\rho \neq \rho'$, the likelihood*

$$p(\mathcal{D} \mid \rho, \alpha) \neq p(\mathcal{D} \mid \hat{\rho}, \hat{\alpha}) \quad (10)$$

for some dataset \mathcal{D} .

Proof in Appendix A.

Without loss of generality, we can choose any set of K context vectors (or word vectors) to fix to have the same result. The identifiability correction allows for direct comparisons between parameter values. In the Bayesian realm, this allows us to calculate for example \hat{R} values to assess convergence to the stationary distribution and effective sample sizes for specific parameters. It also makes it possible to calculate a posterior mean θ , which would otherwise just be zero, as $p(\theta | \mathcal{D}) = p(-\theta | \mathcal{D})$ for any θ .

2.1 COMPARING IDENTIFIED AND NON-IDENTIFIED EMBEDDINGS

Rotation-invariant features are commonly used to analyze word embeddings. These include Euclidean distances between the words (column distances) and cosine similarity (Garg et al., 2018; Eisenstein, 2018; Kozlowski et al., 2019). The co-occurrence probability of any word pair $(w, v) \in W \times W$ is calculated as

$$P(w \wedge v | \theta) = \sigma(\alpha_w^\top \rho_v). \quad (11)$$

Using this, we define the distance between two embeddings as the root mean squared error (RMSE) of the co-occurrence probabilities over all word pairs

$$\text{RMSE}_{co}(\theta, \theta') = \sqrt{\frac{1}{V^2} \sum_{v, w \in W} (P(w \wedge v | \theta) - P(w \wedge v | \theta'))^2} \quad (12)$$

Notably RMSE_{co} is invariant under invertible transformations \mathbf{A} . When $\theta = \theta'$ then $\text{RMSE}_{co}(\theta, \theta') = 0$, but when $\text{RMSE}_{co}(\theta, \theta') = 0$, $\theta' = \begin{bmatrix} \rho \mathbf{A} \\ \alpha \mathbf{A}^{-1} \end{bmatrix}$ for some transformation $\mathbf{A} \in \text{GL}(K)$. Hence, we can compare unidentified as well as identified embeddings. We go on to use it as a similarity metric for two embeddings. This is also the basis of our convergence analysis when true parameters are present. We interpret $\text{RMSE}_{co}(\hat{\theta}, \theta_{true}) = 0$ as the estimate $\hat{\theta}$ having converged to the true parameter θ_{true} .

3 POSTERIOR APPROXIMATION METHODS

We propose two approximation methods for probabilistic word embeddings. Additionally, we show how Laplace approximation can be utilized efficiently for a subset of the vocabulary.

3.1 LAPLACE APPROXIMATION

Laplace approximation of the posterior where it is difficult to sample directly. In Laplace approximation, we approximate the posterior with a multivariate Gaussian distribution around the MAP, i.e.

$$\theta \sim \mathcal{N}(\hat{\theta}_{MAP}, -\mathbf{H}^{-1}(\hat{\theta}_{MAP})), \quad (13)$$

where $\mathbf{H}(\theta)$ is the Hessian matrix of the posterior at θ . To estimate distances between words, we need the covariances of all entries in these word vectors. The most straightforward way to do this would be to calculate the inverse of the Hessian of the posterior at $\hat{\theta}_{MAP}$. For instance, to calculate the credible interval of the distance between ρ_{dog} and ρ_{cat} under the Laplace approximation, only the covariance matrix of $[\rho_{\text{dog}}^\top, \rho_{\text{cat}}^\top]$ is needed. Due to the large parameter space, it is often not possible to invert \mathbf{H} in reasonable time.

Under the word embedding model, it is possible to exploit the sparsity and structure of the Hessian to make Laplace approximation more scalable due to the sparsity of the likelihood and the prior. The structure of the sparse Hessian is further elaborated on in Appendix B.

3.2 GIBBS SAMPLING

For the SGNS likelihood, the distribution of $\rho_w, w \in W$ is, conditionally on α , independent of the other $\rho_{w'}, w' \in W, w' \neq w$. This holds similarly for α_w as well

$$p(\mathcal{D} \mid \rho, \alpha) = \prod_{w \in W} p(\mathcal{D} \mid \rho_w, \alpha) = \prod_{v \in W} p(\mathcal{D} \mid \rho, \alpha_v) \quad (14)$$

Moreover, conditionally on α (or similarly on ρ), the likelihood for ρ is identical to logistic regression when treating α as covariates,

$$p(\mathcal{D} | \rho_w, \alpha) \propto \prod_{v \in W} \sigma(\alpha_v^\top \rho_w)^{n_{wv}^+} \sigma(-\alpha_v^\top \rho_w)^{n_{wv}^-}. \quad (15)$$

Since the distribution of each ρ_v for any $v \in W$ is analogous to the posterior in logistic regression, it is straightforward to construct a Gibbs sampler. The Gibbs sampler alternates sampling ρ and α , where each ρ_v , and each α_v is sampled independently from each other, lending itself well to parallel computation, hence scaling to real-word data sizes. Logistic regression parameters with Gaussian priors can be directly sampled via Polya-Gamma latent variables (Polson et al., 2013). Together, this results in a simple and parallel blocked Gibbs sampler as described in Algorithm 1.

4 EXPERIMENTS

We study the Laplace approximation in Section 3.1 and the Gibbs sampler in Section 3.2, and compare them with current state-of-the-art for estimation, namely MAP estimation, MFVI, and HMC sampling. We use HMC implemented in Stan² and the MFVI algorithm presented by Bamler and Mandt (2017), using the Stan implementation of MFVI (see details in Appendix F). All code is provided on GitHub³.

To study convergence and uncertainty estimates, we use a simulated dataset with known parameters. We complement the simulation experiments with empirical experiments with real data, namely two standard datasets used for embedding methods, the MovieLens dataset (Harper and Konstan, 2015) and the US Congress dataset (Gentzkow et al., 2018).

²<https://mc-stan.org/>

³<https://anonymous.4open.science/r/embedding-uncertainty-estimation-096B/README.md>

Data: $x \in \mathcal{X}$

Hyperparameters: Dimensionality $K \in \mathbb{N}$, vocabulary W , vocabulary size $V = |W|$, number of iterations $N \in \mathbb{N}$, number of Polya-Gamma iterations $S \in \mathbb{N}$

Parameters: $\rho, \alpha \in \mathbb{R}^{V \times K}$

Loss: $\mathcal{L} : \mathcal{X} \times \mathbb{R}^{2V \times K} \rightarrow \mathbb{R} = \sum_{w \in W} \log f_w(\rho_w, \alpha) = \sum_{w \in W} \log g_w(\alpha_w, \rho)$ (SGNS)

for $w \in W$ **do**

$\rho_{w,0} \leftarrow \mathcal{N}(0, 1/K)$
 $\alpha_{w,0} \leftarrow \mathcal{N}(0, 1/K)$

end

for $n \in \{1, \dots, N\}$ **do**

for $w \in W$ **do**

Calculate conditional prior $\mathcal{N}(\mu_{\rho_w}, \Sigma_{\rho_w})$ for ρ_w given ρ_{-w} and α

$\alpha' \leftarrow (\alpha_{v_j}, \dots, \alpha_{v_J})$, where j are the indices where $w_j = w$

$x' \leftarrow (x_j, \dots, x_J)$

$\beta_w \leftarrow \mathcal{N}(0, 1/K)$

for $s \in \{1, \dots, S\}$ **do**

Sample $\omega \sim \text{PolyaGamma}(n_i, \alpha'^\top \beta_w)$

Sample $\beta_w \sim N(\mu_\omega, V_\omega)$, where $V_\omega = (\alpha'^\top \text{diag}(\omega) \alpha' + \Sigma_{\rho_w}^{-1})^{-1}$ and

$\mu_\omega = V_\omega (\alpha'^\top (x_w - 1/2) + \Sigma_{\rho_w}^{-1} \mu_{\rho_w})$

end

$\rho_{w,n} \leftarrow \beta_w$

end

for $w \in W$ **do**

| Sample $\alpha_{w,n}$ with a similar procedure as $\rho_{w,n}$

end

end

Algorithm 1: Gibbs sampling of word embeddings (SGNS)

4.1 SIMULATED DATA

In the simulation study, we use a set of randomly generated word and context vectors. For each $w \in W$, the word and context vectors are simulated from

$$\rho_w \sim \mathcal{N}(0, \frac{\varepsilon^2}{K} \mathbf{I}), \quad \alpha_w \sim \mathcal{N}(0, \frac{\varepsilon^2}{K} \mathbf{I}), \quad (16)$$

where K is the dimensionality of the embedding, and $\varepsilon = 1$ the signal-to-noise ratio. The embedding is scaled inversely to the dimensionality so that the dot products, and thus the signal-to-noise ratio, remain similar in magnitude regardless of the dimensionality K .

We generate random word pairs $(w_i, v_i) \in W \times W$ by sampling uniformly. A Bernoulli random variable, representing whether the pair is a positive or negative sample, X_i is then sampled for $i \in \{1, \dots, N\}$

$$\begin{aligned} (w_i, v_i) &\sim \text{Uniform}(W \times W) \\ X_i &\sim \text{Bernoulli}(\sigma(\alpha_{v_i}^\top \rho_{w_i})) \end{aligned} \quad (17)$$

Each resulting dataset is then estimated with the true K and λ , using MAP estimation, VI, HMC and Gibbs sampler.

In natural language, words often have frequencies proportional to their inverse rank in the vocabulary, i.e. words tend to follow Zipf's law (Zipf, 1935; Piantadosi, 2014). As another experiment, we simulate this by generating w_i and v_i with

$$p(w_i) \propto \frac{1}{\text{rank}(w_i)^a + b}, \quad p(v_i) \propto \frac{1}{\text{rank}(v_i)^a + b}, \quad (18)$$

where $\text{rank}(\cdot)$ is an enumeration of W , and a and b are positive constants. We set $a = 1$ and $b = 2.7$, as suggested by Mandelbrot et al. (1953).

4.1.1 Elimination of Rotational Invariances

As discussed in Section 2, the likelihood can be identified by fixing a submatrix of α . However, any set of K context vectors can be selected, and their values can be set to any

set of linearly independent vectors. In practice, we first find a MAP estimate $\hat{\theta}_{MAP}$, then we set K context vectors to their values during sampling. We found that the selection of words had no effect on the results (see Appendix C), so we used the *last* K context vectors.

In Figure 1, we illustrate how the non-identifiability of the posterior distributions results in rotational symmetries, and then show the effect of identifying the posterior. The marginal posterior of $\rho_{1,1}$ and $\rho_{1,2}$ shows the theorized spherical-shell posterior geometry. The distribution is symmetric around the origin, and has a zero mean. Further we show how restricting $K \times K$ context vectors successfully eliminates the symmetries, simplifying the geometry and making the posterior mean nonzero. Further illustrations of the spherical shell for higher dimensions are provided in Appendix C.

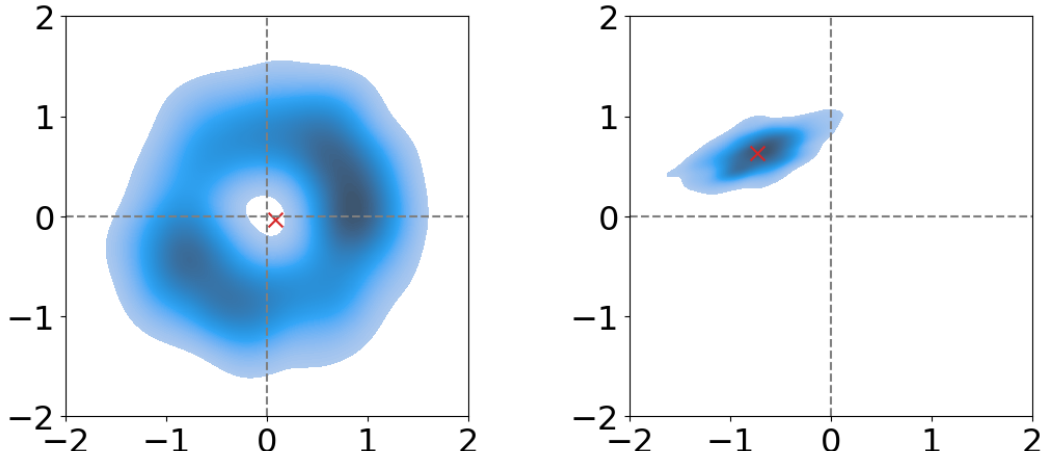


Figure 1: With $K = 2$, the marginal distribution of $\rho_{1,1}$ and $\rho_{1,2}$ displays a circular shell-like symmetry (left), which is eliminated by fixing α_I to a MAP estimate (right). The posterior expectation is marked with a red cross. $N = 2 \cdot 10^4$, $V = 10$. Samples drawn using Stan HMC.

4.1.2 Convergence, Coverage and Effective Sample Size

For the simulated data, we study the convergence of the estimated embeddings $\hat{\theta}$ to the true value θ_{true} . To do this, we use the divergence $RMSE_{co}$ defined in Equation (12).

Figure 2 shows the convergence of the different estimation methods in terms of RMSE_{co} . HMC and the Gibbs sampler perform similarly, while MFVI appears to converge slightly slower as N increases. With small sample sizes, MAP underperforms the other methods, while on large sample sizes it approaches the performance of HMC and the Gibbs sampler. Asymptotically, as expected, HMC, MAP and the Gibbs sampler are very close.

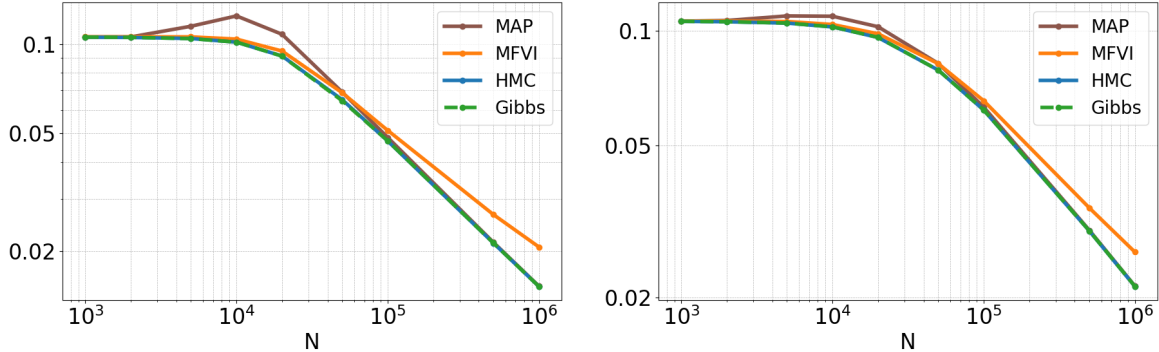


Figure 2: Log-log plotted RMSE_{co} for $K = 5$ and $V = 100$. Averaged over 10 simulated datasets. The left plot shows the results for the uniform simulation the right plot shows the results for the Zipf's law simulation.

As seen in Figures 2 and 3, a loglinear pattern in RMSE_{co} emerges once N is sufficiently large. This is consistent across different values of V and K . Log-log linearity corresponds to $O(N^{-C})$ convergence of RMSE_{co} in terms of N for some positive constant C . For all combinations of K and V , numerical estimates of C were close to -0.5 , i.e. $\text{RMSE}_{co}(N) \approx O(N^{-0.5})$. Since Bayesian point estimates $\hat{\beta}$ approach a $1/\sqrt{N}$ scaled Gaussian as $N \rightarrow \infty$ (Kleijn and Van der Vaart, 2012), the squared error $\mathbb{E}[(\hat{\beta} - \beta)^2]$ is $O(N^{-1})$. Thus its square root is $O(N^{-0.5})$ which matches the convergence rate that we observe for HMC, MAP, and the Gibbs sampler, but interestingly not for MFVI. Moreover, the increase in RMSE_{co} given an increase in V was very close to 1, implying a convergence rate of $O(N^{0.5}/V)$. This also holds for the Zipf-simulated data.

According to Bernstein-von-Mises theorem, under relatively mild assumptions, credible intervals should have valid coverage proportions as the number of observations $N \rightarrow \infty$

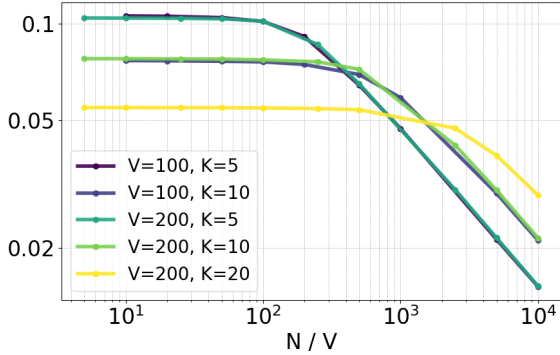


Figure 3: Log-log plotted RMSE_{co} by N/V for the different data sizes, using the Gibbs sampler. Averaged over 10 simulated datasets, uniform simulation.

(Kleijn and Van der Vaart, 2012). Hence, we study the coverage of $P(w \wedge v \mid \theta)$ as a function of data size. The results over all word pairs and 10 simulated datasets are shown in Table 1. HMC and the Gibbs sampler cover the true value roughly 90% of the time regardless of K, V or N . Laplace approximation yields incorrect confidence intervals for small N . This may be both due to an inaccurate normal approximation, and to numerical errors in the inversion and decomposition of the Hessian, something we observed during our experiments. For large values of N , the Laplace approximation confidence intervals approach accurate coverage of 90%, which is expected based on the Bernstein-von-Mises theorem (Kleijn and Van der Vaart, 2012). For MFVI, the confidence intervals are too wide for small values of N , and for large values of N , MFVI only covers the true value under 80.0%-85.0% of the time. This issue worsens as N grows and follows a similar pattern across all combinations of K and V . The tendency of MFVI to underestimate uncertainty is in line with theoretical results on variational inference (Wang and Blei, 2018).

In Table 2 we compare the effective sample size (ESS), as defined via the autocorrelation (Gelman et al., 2013), for HMC and Gibbs. As expected, HMC yields higher effective sample sizes, reaching 89% - 99% of the nominal sample size, while the Gibbs sampler achieves 20-60%, depending on the dataset size. The sampling rates are shown in Table 3. While HMC is faster for small models, the Gibbs sampler outperforms HMC on the two

largest simulation settings. As we will see, running HMC on large datasets is practically not possible due to poor scaling with respect to model and data size.

Finally, we compare the posterior distributions of cosine similarities, a common use case for word embedding in applied settings (Garg et al., 2018; Eisenstein, 2018; Kozlowski et al., 2019). As seen in Figure 4, the posterior distributions of the cosine similarities obtained from HMC and the Gibbs sampler are very similar. However, the posteriors obtained from MFVI differ from these drastically. This is not surprising, due to the use of MFVI posterior approximation, and clearly shows the problem of using MFVI for uncertainty estimation in SGNS embeddings.

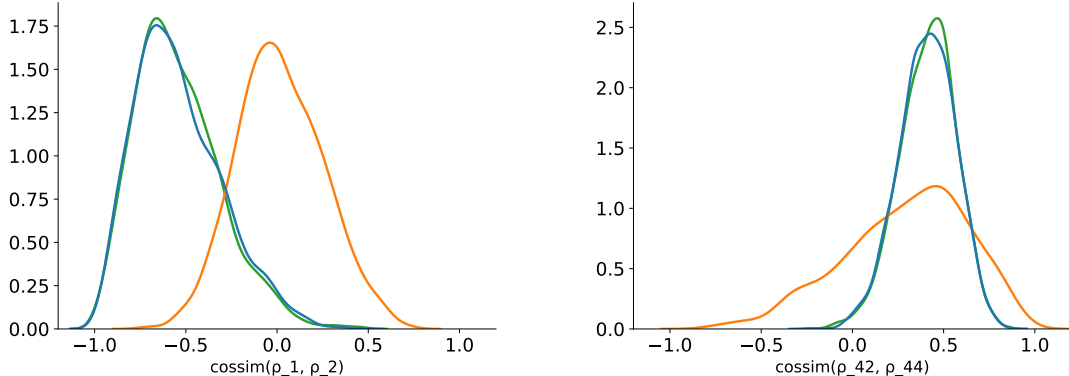


Figure 4: Above: Cosine similarity between ρ_1 and ρ_2 in the first simulated dataset. Below: Cosine similarity between ρ_{42} and ρ_{44} . $K = 5, V = 100, N = 10^5$. Gibbs sampler in green, HMC in blue and MFVI in orange.

4.2 MOVIELENS DATASET

Rudolph et al. (2016) embed the MovieLens data (Harper and Konstan, 2015) using a probabilistic embedding to find thematically similar movies. Following this, we use the MovieLens data as a basis for non-text embedding model experiments. The data contains a collection of numerical movie reviews, which were preprocessed to be suitable for SGNS likelihood in a similarly to Rudolph et al. (2016).

Table 1: Coverage (%) of the true co-occurrence probability $P(w \wedge v \mid \theta_{true})$ of the 90%-credible interval of $P(w \wedge v \mid \theta)$ in the simulated experiment for different data sizes. Averaged over 10 simulated datasets and all word pairs $(w, v) \in W \times W$.

Dataset	Method	1k	2k	5k	10k	20k	50k	100k	500k	1M
$K = 5, V = 100$	HMC	89.9	89.8	89.7	89.7	89.7	89.9	89.9	90.2	89.9
	MFVI	90.2	88.3	84.0	84.5	84.2	85.8	86.6	83.3	79.5
	Gibbs	89.7	89.6	89.7	89.5	89.6	89.9	89.6	90.1	89.7
	Laplace	94.9	94.6	98.6	97.7	96.4	94.9	91.9	90.5	90.3
$K = 10, V = 100$	HMC	90.0	90.0	90.0	90.0	90.0	90.1	90.2	90.0	90.1
	MFVI	92.5	91.9	90.4	88.0	83.7	85.4	85.6	85.1	83.0
	Gibbs	89.9	89.9	89.9	89.9	89.9	89.9	89.6	89.9	90.1
	Laplace	89.9	89.9	89.7	89.4	98.0	96.5	95.2	90.8	90.1
$K = 20, V = 100$	HMC	90.0	89.9	90.0	89.9	90.0	90.0	89.9	89.7	89.9
	MFVI	93.3	93.2	92.8	92.3	90.9	87.3	83.5	85.3	84.5
	Gibbs	89.4	89.4	89.4	89.4	89.4	89.4	89.4	89.7	90.0
	Laplace	79.9	79.9	79.6	79.4	33.6	64.9	95.7	91.1	89.4
$K = 5, V = 200$	HMC	90.2	90.2	90.2	90.3	90.2	90.2	90.1	90.1	90.0
	MFVI	91.5	90.6	87.7	84.0	84.5	83.9	86.2	85.4	83.1
	Gibbs	90.1	90.1	90.1	90.1	90.0	90.0	89.9	89.7	89.9
	Laplace	97.5	97.5	97.8	99.5	98.7	97.9	96.3	91.2	90.5
$K = 10, V = 200$	HMC	88.7	88.8	88.8	88.8	88.9	89.0	89.3	90.4	90.2
	MFVI	92.3	92.1	91.4	90.0	87.4	82.6	84.4	85.6	84.9
	Gibbs	89.5	89.5	89.5	89.6	89.7	89.7	89.7	89.7	89.7
	Laplace	95.0	95.0	95.0	94.6	94.8	99.1	97.9	94.1	91.7
$K = 20, V = 200$	HMC	90.1	90.1	90.2	90.1	90.2	90.2	90.1	90.1	90.1
	MFVI	93.5	93.5	93.5	93.2	92.6	90.5	87.7	85.1	84.4
	Gibbs	90.1	90.1	90.1	90.1	90.1	90.1	90.0	89.8	89.8
	Laplace	89.8	90.0	90.0	89.8	89.8	89.4	94.8	96.5	94.9

Table 2: Median effective sample size, out of 1000 draws after a burn-in of 1000. Simulated data, uniform co-occurrences, $K = 5, V = 100$.

N	1K	2K	5K	20K	50K
HMC	886.6	913.8	931.6	964.3	993.7
Gibbs	579.8	327.9	207.0	286.9	547.7

Table 3: Samples per second for one simulated dataset with uniform co-occurrences. Gibbs results for $S = 10$. Words per second is samples per seconds normalized by V .

Method	N	$K \times V$	Samples/s	Words/s
HMC	$5 \cdot 10^4$	5×100	17.700	1769.9
Gibbs	$5 \cdot 10^4$	5×100	3.333	333.3
HMC	$5 \cdot 10^4$	10×200	4.762	942.4
Gibbs	$5 \cdot 10^4$	10×200	2.467	493.3
HMC	$5 \cdot 10^4$	20×200	2.802	560.4
Gibbs	$5 \cdot 10^4$	20×200	2.233	446.7
HMC	$5 \cdot 10^5$	5×100	2.951	295.1
Gibbs	$5 \cdot 10^5$	5×100	2.900	290.0
HMC	$5 \cdot 10^5$	10×200	2.386	478.0
Gibbs	$5 \cdot 10^5$	10×200	2.880	576.0
HMC	$5 \cdot 10^5$	20×200	0.506	101.2
Gibbs	$5 \cdot 10^5$	20×200	0.733	146.7

Table 4: Samples per second for the MovieLens dataset. Above $K = 20$, $V = 603$, $N = 5 \cdot 10^4$, and below $K = 100$, $V = 603$, $N = 10^6$. Words per second is samples per second normalized by V . Gibbs results for $S = 10$. Runs with an asterisk (*) did not finish before a time limit.

(a) $K = 20$				(b) $K = 100$			
Method	K	Samples/s	Words/s	Method	K	Samples/s	Words/s
HMC	20	0.8333	502.5	HMC	100	< 0.0069*	< 4.19*
Gibbs	20	0.278	167.5	Gibbs	100	0.0267	16.15

MovieLens is a relatively small dataset, allowing us to compare the performance of HMC and the Gibbs sampler. For smaller embedding models ($K = 20$), HMC is still competitive, as shown in Table 4. However, HMC’s efficiency drastically drops as dimensionalities and dataset size increase. HMC only produced a handful of samples before the program was terminated due to hitting the time limit. While the Gibbs sampler also yields significantly less samples per second in these conditions, its performance is still acceptable. It should however be noted that Gibbs sampling benefits from parallel updates, whereas the standard Stan HMC implementation does not.

Table 5: Averaged hold-out log likelihood on the MovieLens data by estimator and sample size. $K = 20$, $\lambda = 1$.

	$\hat{\theta}_{PM\text{-}Gibbs}$	$\hat{\theta}_{MAP}$	$\hat{\theta}_{MFVI}$
$N = 85,000$	-0.7320	-0.7801	-1.1142
$N = 170,000$	-0.6814	-0.7247	-1.1201
$N = 425,000$	-0.6458	-0.6721	-0.8715
$N = 850,000$	-0.6382	-0.6571	-0.6609

Another benefit of using posterior sampling is that we can use the posterior mean as

a point estimates of the word embeddings instead of MAP. In Table 5, we compare the posterior mean estimator $\hat{\theta}_{PM}$ to the MAP estimator $\hat{\theta}_{MAP}$ and the MFVI mean $\hat{\theta}_{MFVI}$ on the MovieLens data. The metric used is the SGNS likelihood on held-out data. On all sample sizes (N), the posterior mean estimator outperforms the MAP estimator.

4.3 US CONGRESS DATASET

For the text data experiment, we use the US Congress speech corpus of Gentzkow et al. (2018), a well-known text dataset popular in the social sciences (Myrick, 2021; Weiss and Zoorob, 2021; Card et al., 2022). We restrict the vocabulary to the 5000 most common words in the dataset, and use a subset of 1 – 10 million words. Further hyperparameters were the window size $M = 2$, and the number of negative samples $n_s = 1$. After this preprocessing, we obtained a sample of 10 million observations. We set $K = 100$ and $\lambda = 1$, common value in applications.

Our experiments are twofold. First, we compare the Gibbs sampler to HMC and MFVI in terms of posteriors of cosine similarities. Furthermore, we compare the VI mean, MAP and HMC and Gibbs sampler posterior mean point estimates in terms of test set hold-out performance. For the larger data sizes, we do not use HMC as it was infeasibly slow.

The posteriors of the cosine similarities between some word pairs are illustrated in Figure 5, on a low dimensionality $K = 50$ where all three algorithms could be run. The Gibbs sampler and HMC yield similar posteriors for this metric. On the other hand, MFVI yields substantially different results from HMC and the Gibbs sampler, both in terms of the posterior mean, and a smaller posterior variance. The latter result is in line with results on MFVI (Wang and Blei, 2018). As seen in Figure 6, the results are similar when $K = 100$. The posteriors are narrower for MFVI than for the Gibbs sampler, and they also differ in means. Since cosine similarity is one of the primary ways of analysis of word embeddings, these differences argue against the use of mean-field approximation for SGNS embeddings.

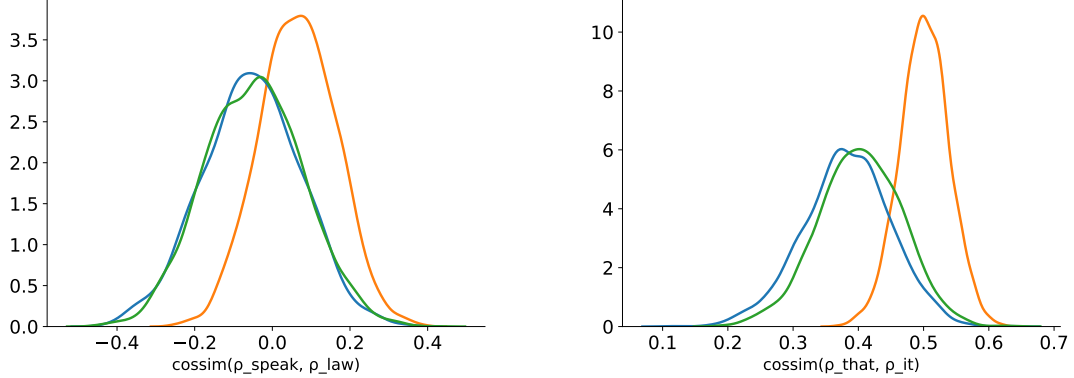


Figure 5: Posterior distribution of the cosine similarity between words for the Gibbs sampler (green), HMC (blue) and MFVI (orange). Left: 'speak' and 'law', right: 'that' and 'it'. $K = 50, N = 500,000$.

Table 6: Hold-out log likelihood on the US Congress data. $K = 50$ on the left, $K = 100$ on the right. $\lambda = 1, M = 2, n_s = 1$. PM-Gibbs is the posterior mean estimator for the Gibbs sampler, PM-HMC is the posterior mean estimator for the HMC sampler.

	(a) $K = 50$			(b) $K = 100$	
	$\hat{\theta}_{PM\text{-}Gibbs}$	$\hat{\theta}_{PM\text{-}HMC}$	$\hat{\theta}_{MAP}$	$\hat{\theta}_{PM\text{-}Gibbs}$	$\hat{\theta}_{MAP}$
$N = 10^5$	-0.7648	-0.7584	-0.8927	-0.7374	-0.8209
$N = 5 \cdot 10^5$	-0.7556	-0.7574	-0.8648	-0.7136	-0.7836
$N = 10^6$	-0.72549	-0.7374	-0.7896	-0.6594	-0.6948
$N = 5 \cdot 10^6$	-0.6551	NA	-0.6625	-0.6360	-0.6357

Finally, Table 6 presents the results of the hold-out performance experiment on the US congress data. On both $K = 50$ and $K = 100$, both posterior mean estimators outperform the MAP estimator. However, on the full training data $N = 10^7$, MAP is, as expected, on par with the posterior mean point estimator. On $K = 50$, where we can compare the posterior mean estimators from HMC and the Gibbs sampler, they perform similarly.

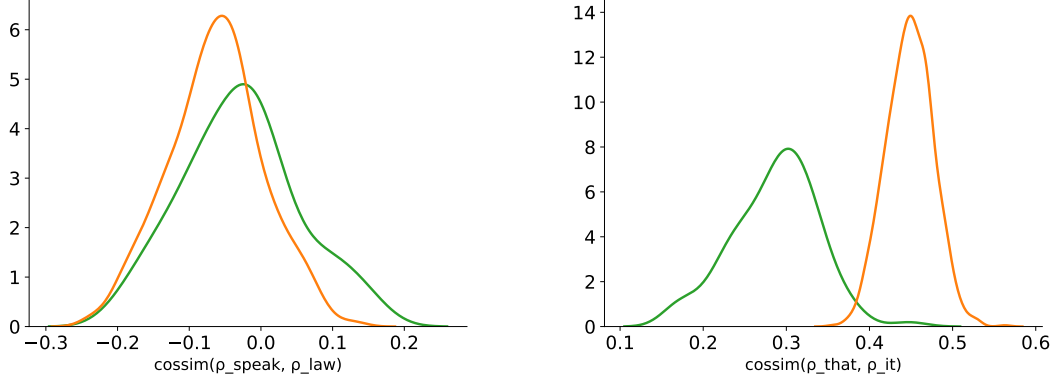


Figure 6: Posterior distribution of the cosine similarity between words for the Gibbs sampler (green) and MFVI (orange). Left: 'speak' and 'law', right: 'that' and 'it'. $K = 100, N = 500,000$.

5 CONCLUSION

In this paper, we showed that the undesirable symmetries in SGNS embeddings persist despite the previous efforts to eliminate them. We then proposed a simple way to eliminate the symmetries and identify the SGNS model. This allows for full use of \hat{R} and the effective sample size, and makes the posterior mean a reasonable point estimate.

On simulated data, we showed that the current standard method for estimating probabilistic SGNS, MFVI, yields inaccurate credible intervals, especially on large data. We also showed that HMC and the Gibbs sampler yield accurate credible intervals, and Laplace approximation yields accurate credible intervals on larger sample sizes.

On real data, we demonstrated that MFVI and the Gibbs sampler yield different posterior distributions of cosine similarities, which are one of the primary metrics used in word embeddings. This suggests that MFVI is not a good approximation for SGNS embeddings in terms of uncertainty estimates. We also showed that the Gibbs sampler is computationally feasible in this setting, while Stan HMC is not. Finally, we showed that the new posterior mean estimator outperformed the MAP and VI mean estimators.

Data Availability Statement

The data that support the findings of this study are openly available in the *MovieLens* data repository at <https://grouplens.org/datasets/movielens/>, as well as the *Congressional Record for the 43rd-114th Congresses: Parsed Speeches and Phrase Counts* data at https://data.stanford.edu/congress_text.

References

Abramson, C. M., Z. Li, T. Prendergast, and M. Sánchez-Jankowski (2024). Inequality in the origins and experiences of pain: What “big (qualitative) data” reveal about social suffering in the united states. *RSF: The Russell Sage Foundation Journal of the Social Sciences* 10(5), 34–65.

Antoniak, M. and D. Mimno (2018). Evaluating the stability of embedding-based word similarities. *Transactions of the Association for Computational Linguistics* 6, 107–119.

Bamler, R. and S. Mandt (2017). Dynamic word embeddings. In *International conference on Machine learning*, pp. 380–389. PMLR.

Bickel, P. J. and K. A. Doksum (2015). *Mathematical statistics: basic ideas and selected topics*, Volume 1. Chapman and Hall/CRC.

Bodell, M. H., M. Arvidsson, and M. Magnusson (2019). Interpretable word embeddings via informative priors. *arXiv preprint arXiv:1909.01459*.

Card, D., S. Chang, C. Becker, J. Mendelsohn, R. Voigt, L. Boustan, R. Abramitzky, and D. Jurafsky (2022). Computational analysis of 140 years of us political speeches reveals more positive but increasingly polarized framing of immigration. *Proceedings of the National Academy of Sciences* 119(31), e2120510119.

Eisenstein, J. (2018). Natural language processing. *Jacob Eisenstein 507*.

Garg, N., L. Schiebinger, D. Jurafsky, and J. Zou (2018). Word embeddings quantify 100 years of gender and ethnic stereotypes. *Proceedings of the National Academy of Sciences 115*(16), E3635–E3644.

Gelman, A., J. B. Carlin, H. S. Stern, D. B. Dunson, A. Vehtari, and D. B. Rubin (2013). *Bayesian Data Analysis*. CRC Press.

Gentzkow, M., J. M. Shapiro, and M. Taddy (2018). Congressional record for the 43rd-114th congresses: Parsed speeches and phrase counts. In *URL: <https://data.stanford.edu/>*.

Harper, F. M. and J. A. Konstan (2015). The movielens datasets: History and context. *Acm transactions on interactive intelligent systems (tiis) 5*(4), 1–19.

Kleijn, B. J. and A. W. Van der Vaart (2012). The bernstein-von-mises theorem under misspecification.

Kozlowski, A. C., M. Taddy, and J. A. Evans (2019). The geometry of culture: Analyzing the meanings of class through word embeddings. *American Sociological Review 84*(5), 905–949.

Mandelbrot, B. et al. (1953). An informational theory of the statistical structure of language. *Communication theory 84*, 486–502.

Mikolov, T., I. Sutskever, K. Chen, G. S. Corrado, and J. Dean (2013). Distributed representations of words and phrases and their compositionality. *Advances in neural information processing systems 26*.

Mu, C., G. Yang, and Y. Zheng (2019). Revisiting skip-gram negative sampling model with rectification. In *Intelligent Computing: Proceedings of the 2019 Computing Conference, Volume 1*, pp. 485–497. Springer.

Myrick, R. (2021). Do external threats unite or divide? security crises, rivalries, and polarization in american foreign policy. *International Organization* 75(4), 921–958.

Pennington, J., R. Socher, and C. D. Manning (2014). Glove: Global vectors for word representation. In *Proceedings of the 2014 conference on empirical methods in natural language processing (EMNLP)*, pp. 1532–1543.

Piantadosi, S. T. (2014). Zipf’s word frequency law in natural language: A critical review and future directions. *Psychonomic bulletin & review* 21, 1112–1130.

Polson, N. G., J. G. Scott, and J. Windle (2013). Bayesian inference for logistic models using pólya–gamma latent variables. *Journal of the American statistical Association* 108(504), 1339–1349.

Rodman, E. (2020). A timely intervention: Tracking the changing meanings of political concepts with word vectors. *Political Analysis* 28(1), 87–111.

Rudolph, M. and D. Blei (2017). Dynamic Bernoulli embeddings for language evolution. *arXiv preprint arXiv:1703.08052*.

Rudolph, M., F. Ruiz, S. Athey, and D. Blei (2017). Structured embedding models for grouped data. *Advances in neural information processing systems* 30.

Rudolph, M., F. Ruiz, S. Mandt, and D. Blei (2016). Exponential family embeddings. *Advances in Neural Information Processing Systems* 29.

Vallebueno, A., C. Handan-Nader, C. D. Manning, and D. E. Ho (2024). Statistical uncertainty in word embeddings: Glove-v. *arXiv preprint arXiv:2406.12165*.

Wang, Y. and D. M. Blei (2018). Frequentist consistency of variational Bayes. *Journal of the American Statistical Association*.

Weiss, M. and M. Zoorob (2021). Political frames of public health crises: Discussing the opioid epidemic in the us congress. *Social Science & Medicine* 281, 114087.

Yrjänäinen, V. and M. Magnusson (2022). Probabilistic embeddings with laplacian graph priors. *arXiv preprint arXiv:2204.01846*.

Zipf, G. K. (1935). The psychobiology of language.

A Proofs

Proposition 1. *Given any embedding $\hat{\alpha}, \hat{\rho}$, and any invertible matrix $\mathbf{M} \in \mathbb{R}^{K \times K}$, the following embedding*

$$\rho = \hat{\rho}(\hat{\alpha}_I^{-1}\mathbf{M})^{-\top}, \quad \alpha = \begin{bmatrix} \mathbf{M} \\ \hat{\alpha}_J\hat{\alpha}_I^{-1}\mathbf{M} \end{bmatrix} \quad (8)$$

has the same likelihood

$$p(\mathcal{D} \mid \rho, \alpha) = p(\mathcal{D} \mid \hat{\rho}, \hat{\alpha}) \quad (9)$$

for any dataset \mathcal{D} .

PROOF 1. For any data \mathcal{D} , the likelihood is a function of the product $\alpha\rho^\top$

$$p(\mathcal{D} \mid \rho, \alpha) \equiv g(\alpha\rho^\top) \quad (19)$$

which in turn means that

$$\alpha\rho^\top = \alpha'(\rho')^\top \implies p(\mathcal{D} \mid \rho, \alpha) = p(\mathcal{D} \mid \rho', \alpha') \quad (20)$$

for any data \mathcal{D} . Thus, we need to show that the matrices $\alpha\rho^\top$ and $\hat{\alpha}\hat{\rho}^\top$ are always equal

$$\alpha\rho^\top = \begin{bmatrix} \mathbf{M} \\ \hat{\alpha}_J\hat{\alpha}_I^{-1}\mathbf{M} \end{bmatrix} (\hat{\rho}(\hat{\alpha}_I^{-1}\mathbf{M})^{-\top})^\top = \begin{bmatrix} \mathbf{M} \\ \hat{\alpha}_J\hat{\alpha}_I^{-1}\mathbf{M} \end{bmatrix} (\hat{\alpha}_I^{-1}\mathbf{M})^{-1}\hat{\rho} \quad (21)$$

$$= \begin{bmatrix} \mathbf{M} \\ \hat{\alpha}_J\hat{\alpha}_I^{-1}\mathbf{M} \end{bmatrix} \mathbf{M}^{-1}\hat{\alpha}_I\hat{\rho}^\top = \begin{bmatrix} \mathbf{M}\mathbf{M}^{-1}\hat{\alpha}_I \\ \hat{\alpha}_J\hat{\alpha}_I^{-1}\mathbf{M}\mathbf{M}^{-1}\hat{\alpha}_I \end{bmatrix} \hat{\rho}^\top = \begin{bmatrix} \hat{\alpha}_I \\ \hat{\alpha}_J \end{bmatrix} \hat{\rho}^\top = \hat{\alpha}\hat{\rho}^\top \quad (22)$$

and thus $p(\mathcal{D} \mid \hat{\rho}, \hat{\alpha}) \equiv p(\mathcal{D} \mid \rho, \alpha)$. \square

Proposition 2. *Given any invertible matrix $\mathbf{M} \in \mathbb{R}^{K \times K}$, any two embeddings $\alpha = \begin{bmatrix} \mathbf{M} \\ \alpha_J \end{bmatrix}, \rho$ and $\alpha' = \begin{bmatrix} \mathbf{M} \\ \alpha'_J \end{bmatrix}, \rho'$, for which $\alpha \neq \alpha'$ or $\rho \neq \rho'$, the likelihood*

$$p(\mathcal{D} \mid \rho, \alpha) \neq p(\mathcal{D} \mid \hat{\rho}, \hat{\alpha}) \quad (10)$$

for some dataset \mathcal{D} .

PROOF 2.

$$\theta \neq \theta' \implies p(\mathcal{D} \mid \theta) \neq p(\mathcal{D} \mid \theta') \quad (23)$$

By contraposition, this is equivalent to

$$p(\mathcal{D} \mid \theta') = p(\mathcal{D} \mid \theta) \implies \theta = \theta' \quad (24)$$

The likelihood is a function of the product

$$p(\mathcal{D} \mid \theta) \equiv g(\alpha \rho^\top) \quad (25)$$

which means that two likelihoods are identical for any data \mathcal{D} iff $\alpha \rho^\top = \hat{\alpha} \hat{\rho}^\top$. Given that $\alpha_I = \hat{\alpha}_I = \mathbf{M}$, the equality becomes

$$\alpha \rho^\top = \begin{pmatrix} \alpha_I \rho_I^\top & \alpha_I \rho_J^\top \\ \alpha_1 \rho_I^\top & \alpha_1 \rho_J^\top \end{pmatrix} = \begin{pmatrix} \hat{\alpha}_I \rho_I^\top & \hat{\alpha}_I \rho_J^\top \\ \alpha_1 \rho_I^\top & \alpha_1 \rho_J^\top \end{pmatrix} = \begin{pmatrix} \hat{\alpha}_I \hat{\rho}_I^\top & \hat{\alpha}_I \hat{\rho}_J^\top \\ \hat{\alpha}_1 \hat{\rho}_I^\top & \hat{\alpha}_1 \hat{\rho}_J^\top \end{pmatrix} \quad (26)$$

Since α_I^{-1} exists

$$\hat{\alpha}_I \rho_I^\top = \hat{\alpha}_I \hat{\rho}_I^\top \implies \rho_I = \hat{\rho}_I \quad (27)$$

$$\hat{\alpha}_I \rho_J^\top = \hat{\alpha}_I \hat{\rho}_J^\top \implies \rho_J = \hat{\rho}_J \quad (28)$$

and thus

$$\alpha_J \hat{\rho}_I^\top = \hat{\alpha}_J \hat{\rho}_I^\top \implies \alpha_J = \hat{\alpha}_J \quad (29)$$

i.e., $\rho = \hat{\rho}$ and $\alpha = \hat{\alpha}$. \square

B Structure of the Hessian

As seen in Equation (3), the skip-gram likelihood factors into terms with only a few parameters. Generally, in natural text corpora, most of the possible word pairs do not appear

together. Consequently, the interactions between words are inherently sparse. This means that most of the entries in the Hessian are going to be zero (for the positive samples). For example, in a random 50 million token subset of Wikipedia, roughly 0.25% of the word pairs actually co-occur within a window size of 5. The sparsity is illustrated in Figure 7. We can leverage this property to improve computations of the Hessian.

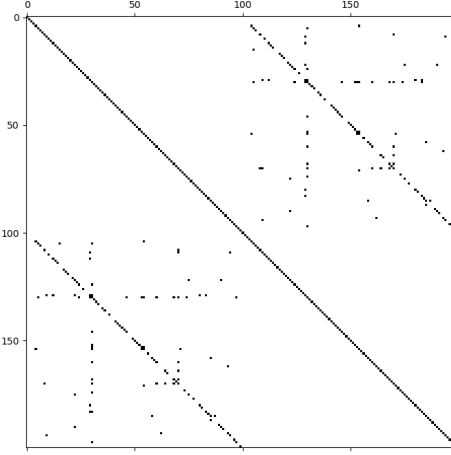


Figure 7: Nonzero elements of the Hessian matrix for a subset of 100 word and 100 context vectors in a model. Data from 50M token Wikipedia subset, standard preprocessing by Mikolov et al. (2013) was used.

The Hessian of the positive samples also factors into submatrices consisting of outer products

$$\frac{\partial^2}{\partial^2 \rho_w} \log p(\mathcal{D} \mid \theta)^+ = - \sum_{v \in W} \alpha_v \alpha_v^\top \sigma'(\rho_w^\top \alpha_v) n_{v,w}^+ \quad (30)$$

for the diagonal blocks, and for the off-diagonal blocks

$$\frac{\partial^2}{\partial \rho_w \partial \alpha_v} \log p(\mathcal{D} \mid \theta)^+ = -\rho_w \alpha_v^\top \sigma'(\rho_w^\top \alpha_v) n_{w,v}^+ - I \sigma(\rho_w^\top \alpha_v) n_{w,v}^+ \quad (31)$$

$$\frac{\partial^2}{\partial \rho_w \partial \rho_v} \log p(\mathcal{D} \mid \theta)^+ = \mathbf{0} \quad (32)$$

$$\frac{\partial^2}{\partial \alpha_w \partial \alpha_v} \log p(\mathcal{D} \mid \theta)^+ = \mathbf{0} \quad (33)$$

where the positive samples $n_{w,v}^+$ will often be 0. Since the derivative of the logistic function $\sigma'(\cdot)$ is a symmetric function, the same formulas hold for the negative samples as well.

Note that the diagonal submatrices are low-rank if there are less than K co-occurring word types, and the off-diagonal submatrices are always rank 1 or 0.

C Additional Results

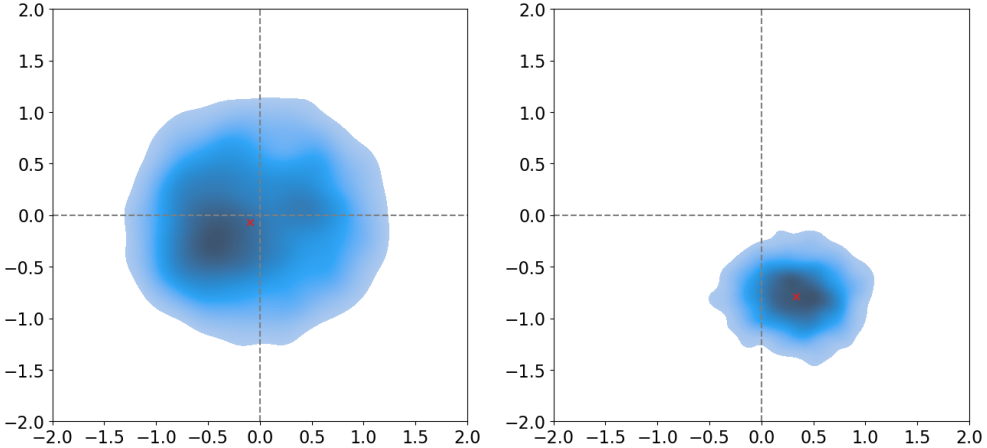


Figure 8: $\rho_{4,1}$ and $\rho_{4,2}$ for $K = 5$, $V = 100$, $N = 50,000$. The left figure demonstrates the rotational symmetry which is eliminated by fixing α_I to a MAP estimate, shown in the right figure.

In higher dimensions than $K = 2$, the hypersphere resulting from the orthogonal symmetries \mathbf{O} is not a circle, but a sphere or a hypersphere instead. Hence, the 2D projection of the circular shell is closer to standard Gaussian than a torus, as in the $K = 2$ case. The symmetries for $K = 5$ are illustrated in Figure 8.

To check the sensitivity of the results to the rotational fix, we calculated posteriors for the cosine similarity of some word vector pairs. In one run, we fixed the last K context vectors as we do in the article. In another run, K words were selected randomly from the vocabulary and their corresponding context vectors were fixed to the values of the MAP estimate. The results are shown in Figure 9. Visually, the resulting posteriors are very similar. Moreover, the \hat{R} measures were very close to 1: $\hat{R} = 1.0012$ for both inspected word pairs, which is an indication of no difference between the two approaches.

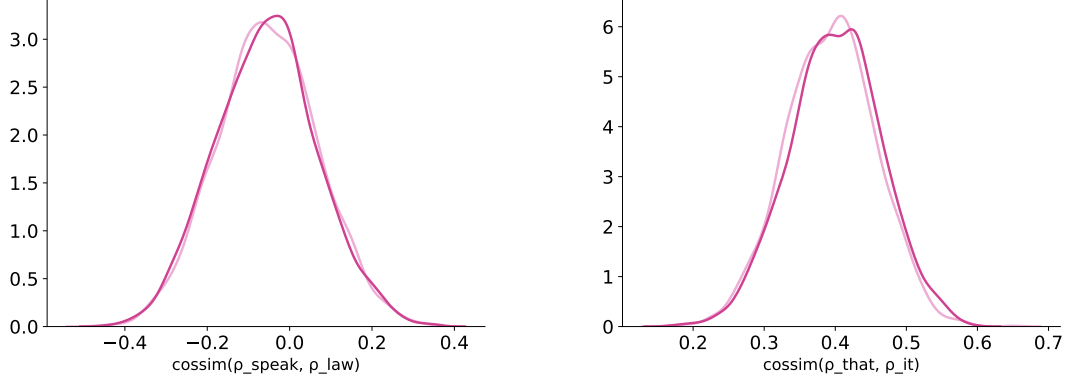


Figure 9: Posterior distribution of the cosine similarity between words. In dark, a Gibbs sampler with the last K context vectors fixed, and in light, randomly selected K words fixed to a MAP estimate. Left: 'speak' and 'law', right: 'that' and 'it'. $K = 50, N = 500,000, K = 50$.

D Laplace Approximation Implementation

The Laplace approximation was implemented in the following steps

1. Find the MAP estimate $\hat{\theta}_{MAP}$
2. Calculate the Hessian $\mathbf{H}(\theta)$
3. Invert the Hessian $\mathbf{H}(\theta)$ at $\hat{\theta}_{MAP}$ and set the covariance $\Sigma = \mathbf{H}(\hat{\theta}_{MAP})^{-1}$
4. Calculate the conditional covariance Σ' given that $\alpha_I = \hat{\alpha}_I$
5. Find the eigendecomposition of $\Sigma' = UDU^{-1}$
6. Sample from $\theta \approx U\sqrt{D}\varepsilon$, where ε is a vector of standard Gaussians. If some of the values of D are negative due to numerical errors, set them to zero.

The Cholesky decomposition failed due to the covariance not being numerically positive-definite. The eigendecomposition was used to find the closest numerically positive-definite

decomposition $L^T L \approx \Sigma'$. An alternative approach using pairwise covariances was also tested. After steps 1-4,

1. For sampling ρ_w and α_v , formulate the covariance matrix $\Sigma_{\rho,\alpha} = \begin{bmatrix} \Sigma_{w,w} & \Sigma_{w,v} \\ \Sigma_{v,w} & \Sigma_{v,v} \end{bmatrix}$
2. Sample $\begin{bmatrix} \rho_w \\ \alpha_v \end{bmatrix}$ from $\mathcal{N}(\begin{bmatrix} \hat{\rho}_w \\ \hat{\alpha}_v \end{bmatrix}, \Sigma_{\rho,\alpha})$ via the Cholesky decomposition

The pairwise covariance matrices displayed less numerical issues, and the standard Cholesky decomposition could be used. The pairwise approach yielded similar results on the coverage experiment, albeit being slower.

E MFVI, MAP and HMC Implementation

We implemented MFVI, MAP estimation, HMC using Stan. Specifically, we used `cmdstanpy` for MFVI and MAP, and `pystan` for HMC. See Listing 1 for the unconstrained model and Listing 2 for the constrained version, where we constrain the K last context embeddings. Note that `lambda` used here denotes the standard deviation of the priors. We utilize the aggregated formulation of the likelihood, described by Equation 5.

For MFVI we use Stan's default settings with 5000 iterations for optimization and draw 2000 posterior samples. For MAP estimation, we use Stan's optimization routine, with the default optimization algorithm L-BFGS. For HMC we use 2 chains, each with 1000 burn-in and 2000 drawn samples.

All preprocessing and postprocessing was done in Python.


```
32     } else {
33
34         target += counts[u] * log_inv_logit(-l_contribution);
35     }
36 }
```

Listing 1: Stan model for probabilistic skip-gram negative sampling

```

25         context_vectors[v, k] = context_vectors_raw[v, k];
26     }
27 }
28
29 for (v in (V-K+1):V) {
30     for (k in 1:K) {
31         // row index in fixed_context_matrix is (v - (V-K))
32         context_vectors[v, k] = fixed_context_matrix[v - (V - K), k];
33     }
34 }
35 }
36
37 model {
38
39     // Only apply priors to the unconstrained the context vectors:
40     for (v in 1:(V-K)) {
41         for (k in 1:K) {
42             context_vectors_raw[v, k] ~ normal(0, lambda);
43         }
44     }
45
46     for (v in 1:V) {
47         for (k in 1:K) {
48             word_vectors[v, k] ~ normal(0, lambda);
49         }
50     }
51
52     for (u in 1:U) {
53         real l_contribution = dot_product(
54             word_vectors[target_word[u]],
55             context_vectors[context_word[u]]
56         );

```

```

57     if (posneg_labels[u] == 1) {
58
59         target += counts[u] * log_inv_logit(l_contribution);
60
61     } else {
62
63         target += counts[u] * log_inv_logit(-l_contribution);
64     }
65 }

```

Listing 2: Stan model for probabilistic skip-gram negative samples with K constrained context embeddings

F Gibbs sampler Implementation

The Gibbs sampler was implemented in Python using the TensorFlow framework and the `probabilistic_word_embeddings` PyPi package⁴.

The Gibbs sampler was parallelized within iterations. Specifically, while sampling the word vectors ρ_w , 100 vectors were sampled at once. The matrix products, such as $\alpha'^\top \text{diag}(\omega)$, matrix inversions and other matrix and vector operations were all implemented in TensorFlow the 100 parallelized words at a time. Moreover, sampling from the multivariate Gaussian was done via the Cholesky decomposition, using a parallelized implementation from TensorFlow

$$L_w L_w^T = V_{\omega, w} \text{ (via Cholesky)} \quad (34)$$

$$\beta_w = L_w \varepsilon_w + \mu_\omega \quad (35)$$

$$\varepsilon_w \sim \mathcal{N}(0, \mathbf{I}) \quad (36)$$

For the Polya-Gamma distribution, the CPU-based `polyagamma` PyPi package⁵ was used. Otherwise random variables were generated with TensorFlow.

⁴(https://pypi.org/project/probabilistic_word_embeddings/)

⁵(<https://pypi.org/project/polyagamma/>)

G Computational Complexity

The Gibbs sampler consists of six steps which are not negligible in terms of computational cost. The sampling cost per word can be expressed in terms of the dimensionality K , number of unique co-occurring words n_u , and the number of Polya-Gamma steps S .

1. Initialization sampling – $O(K)$
2. Polya-Gamma random variable sampling – $O(S \cdot n_u)$ (CPU)
3. Calculating the precision matrix V_ω^{-1} – $O(S \cdot n_u \cdot K^2)$
4. Inverting the precision matrix to find V_ω – $O(S \cdot K^3)$
5. Cholesky decomposition V_ω – $O(S \cdot K^3)$
6. Sampling the vectors $\rho \sim \mathcal{N}(\mu, V_\omega)$ – $O(S \cdot K^2)$

To get the full complexity, most of these are just multiplied by the vocabulary size V . However, n_u depends on the specific word. However, it occurs as a linear term, so $O(n_u \cdot V)$ evaluates to $O(N_u)$, where N_u is the total number of unique word pairs in the data.

Thus, the total asymptotic complexity can be dominated by one of the following three factors

1. Polya-Gamma random variable sampling – $O(S \cdot N_u)$ (when the CPU dominates)
2. Calculating the precision matrix V_ω^{-1} – $O(S \cdot N_u \cdot K^2)$
3. Inverting and decomposing the precision matrix – $O(S \cdot V \cdot K^3)$

In practice, the `polyagamma` package seems to be fast enough that the total complexity is

$$O(S \cdot N_u \cdot K^2 + S \cdot V \cdot K^3) \tag{37}$$

Note that by definition, $N_u \leq V^2$.